Acta Crystallographica Section A
Foundations of Crystallography
ISSN 0108-7673

Received 3 December 2008
Accepted 29 January 2009

Crystal topologies – the achievable and inevitable symmetries

Georg Thimm

Mechanical and Aerospace Engineering, Nanyang Technological University, 50 Nanyang Avenue, Singapore 639798, Singapore. Correspondence e-mail: mgeorg@ntu.edu.sg

The link between the crystal topology and symmetry is examined, focusing on the conditions under which a structure with a given topology can exhibit a certain symmetry. By defining embeddings for quotient graphs (finite representations of crystal topologies) and the corresponding nets (the graph-theoretical equivalents of structures), a strong relationship between the automorphisms of the quotient graphs and the symmetry of the embedded net is established. This allows one to constrain the relative node positions under the premise that an embedding of a net has a certain symmetry, and allows one to assign nodes to equivalents of Wyckoff positions. Two-dimensional examples as well as known crystal structures are used to illustrate the findings. A comparison with a related publication and a discussion on whether constraints on distances between atoms and on bond angles result in restrictions on symmetry without causing confusion conclude the work.

1. Introduction

Structures with the same topology exhibit an apparent preference for symmetries in certain space groups. For example, garnet structures possess the same or similar symmetries for a wide range of compositions. Another example is provided by the high- and low-temperature phases of quartz: the high-temperature phases exhibit the symmetries of space groups $P6_222$ and $P6_422$. These transform displacively (*via* an intermediate incommensurate phase) into $P3_121$ and $P3_221$, respectively, at low temperatures, where the space groups of the low-temperature phases are subgroups of the space groups of the high-temperature phases (Heany, 1994). Visual examination of a pair of such related structures invites speculations about the causes of these similarities: the preserved connectivity or topology. Indeed, it has been shown that a close relationship exists between the topology of a net (that is, the graph-theoretical, dimensionless representation of a structure) and the maximal symmetry a structure of a given topology can assume (Eon, 1999; Grosse-Kunstleve, 1999; Delgado-Friedrichs & O'Keeffe, 2003; Klee, 2004; Thimm & Winkler, 2006). However, this observation is not quite satisfying as it leaves open questions:

(1) Can a net be embedded (coordinates assigned to nodes) in such a way that a chosen symmetry is observable?

(2) Under what conditions is a given symmetry realized or realizable?

(3) For a given net, do symmetries exist that defy displacive phase transitions?

The following discussion of the copper structure further motivates these questions, which have already been addressed by Blatov (2007) and Baburin & Blatov (2007) for selected classes of structures only. Here no such restriction is made.

The work presented by Eon (1999) has a certain similarity with the approach proposed here. As the notation, mathematical tools and approach used are different enough to disallow a one-to-one comparison, §7 compares the two approaches.

2. An informal discussion: copper

Copper crystallizes in $Fm\bar{3}m$ [Cu at (0, 0, 0) and a = 3.615 Å (Downs & Hall-Wallace, 2003); space-group symbols follow *International Tables for Crystallography* Volume A (Hahn, 1992)]. Each atom has 12 nearest neighbours at a distance of 2.5562 Å. The structure has one atom in a primitive cell. One may ask whether lower-symmetry *translationengleiche* embeddings of this net can exist, and if so, which symmetries they have.

It is obvious that a displacive and *translationengleiche* phase transition of copper cannot exist if a cubic (primitive) unit cell is maintained. Consequently, the only way to reduce the symmetry is to change the shape of the unit cell. A hypothetical phase transition (through an non-uniform strain, although this is unlikely to be observed in nature) can only lead to space groups that are subgroups of $Fm\bar{3}m$ but outside the cubic system. Among many others, the space groups $I4/mmm$ and $P1$ are *translationengleiche* subgroups of $Fm\bar{3}m$. That $I4/mmm$ is possible is obvious: it is sufficient to change the length of the cubic cell in the direction of the c axis. However, $P1$ seems impossible: placing the Cu atom in a triclinic cell results in a structure with symmetry $P\bar{1}$ (for any chosen origin).

Now, without reference to an existing structure, consider a structure in which each copper atom is bonded to an additional, singly coordinated atom. These atoms considerably change the symmetry. For example, an axis of rotational symmetry is necessarily parallel to the bond linking the added atom to the rest of the net and an inversion symmetry is forbidden. Therefore, the 'augmented' structure cannot have the same translational symmetry as copper and have cubic symmetry. However, the theory presented in Thimm & Winkler (2006) stipulates cubic symmetry (the additional nodes are not parts of a cycle).

Adding a second set of singly bonded atoms changes the maximal possible symmetry again: an inversion is again possible.

Some of the reasons for the symmetry of the embedding of a net being reduced with respect to the symmetry, as proposed by Thimm & Winkler (2006), are:

(1) changing the cell parameters, which leads to a *translationengleiche* space group;

(2) changing the volume of the unit cell, which leads to a non-*translationengleiche* and possibly non-*klassengleiche* symmetry;

(3) nodes are moved away from the Wyckoff positions they occupy in a maximal-symmetry embedding, inducing a non-*klassengleiche* symmetry;

(4) the presence of singly connected nodes;

(5) the ideal symmetry constrains

(*a*) several nodes to be on the same (Wyckoff) position,

(*b*) nodes onto positions coinciding with edges, or

(*c*) nodes or edges into positions with physically meaningless distances or angles to each other (see §8).

3. Crystals, nets, quotient graphs and embeddings

The conventional approach to defining quotient graphs [see Chung *et al.* (1984) and Klein (1996)] lacks the notion of independence of node positions under mathematical reasoning. Therefore, Cohen & Megiddo (1991) and Thimm & Winkler (2006) proposed an alternative definition of nets and quotient graphs which is independent of an embedding or structures. In this definition, quotient graphs (QGs) are first defined as a set of labelled graphs, and only then are the nets defined as a cross product of a quotient graph and an integer vector space. An embedding is then essentially an assignment of coordinates to nodes in the quotient graph and a choice of basis vectors (details are given later). This section complements this definition with observations related to symmetries.

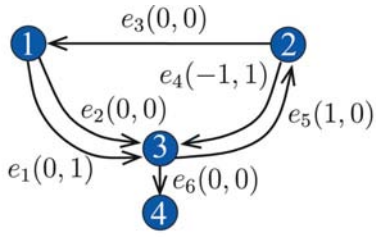

$\mathcal{E}(e_1) = (0.3, 0.5)$ $\mathcal{E}(e_2) = (0.3, -0.5)$
$\mathcal{E}(e_3) = (0.3, 0.0)$ $\mathcal{E}(e_4) = (-0.4, 0.5)$
$\mathcal{E}(e_5) = (0.4, 0.5)$ $\mathcal{E}(e_6) = (-0.5, 0.0)$

Figure 1
$\mathbf{Q}^{\mathrm{L}}$ and an embedding $\mathcal{E}$.

In Thimm & Winkler (2006), a *quotient graph* $\mathbf{Q}$ of dimension D is defined as a finite graph consisting of N nodes $\mathbf{Q}_N = \{n_i | 1 \leq i \leq N\}$ and directed, labelled edges $\mathbf{Q}_E = \{e = (n_i \overset{\mathbf{v}}{\rightarrow} n_j)\} \subset \mathbf{Q}_N \times \mathbb{Z}^D \times \mathbf{Q}_N$ with dimension $D \geq 1$. An edge $e = (n_i \overset{\mathbf{v}}{\rightarrow} n_j)$ is identical to the edge $\overline{e} = (n_j \overset{-\mathbf{v}}{\longrightarrow} n_i)$. The bar over the symbol for the edge is to distinguish between the orientation of the two representations. To avoid notational complexity, the latter notation shall only be used when edge orientations matter.

A net $\mathbf{G} = \langle \mathbf{Q}, \mathbb{Z}^D \rangle$ is defined as the cross product of a quotient graph $\mathbf{Q}$ of dimension D and an integer vector space of the same dimension. In this cross product

$$\mathbf{G}_N = \left\{ n_i(\mathbf{x}) | 1 \leq i \leq N, \mathbf{x} \in \mathbb{Z}^D \right\}$$

is the set of nodes in $\mathbf{G}$ and

$$\mathbf{G}_E = \left\{ n_i(\mathbf{x}) \leftrightarrow n_j(\mathbf{x} + \mathbf{v}) \; | e = \left(n_i \overset{-\mathbf{v}}{\rightarrow} n_j \right) \in \mathbf{Q}_E, \mathbf{x} \in \mathbb{Z}^D \right\}$$

is the set of (undirected) edges. Hereby, a net is defined without recourse to an embedding (or a crystal structure), cell parameters or atom positions.

For the purpose of creating a link between the dimensionless crystal topology as described by a QG or a net (the graph-theoretical equivalent of a structure), the embeddings of QGs and nets are defined in the following. Superficially, an embedding of a quotient graph is obtained from an assignment of relative positions (relative atom positions in fractional coordinates for a crystal structure).

Definition 3.1. Embedding of a QG. An embedding $\mathcal{E}$ of a QG is a function $\mathbf{Q}_E \rightarrow \mathbb{R}^D$ with $\mathcal{E}(\overline{e}) = -\mathcal{E}(e)$ such that $\mathcal{E}$ is consistent: for all cycles c in the QG

$$\sum_{e \in c} \mathbf{v} = \sum_{e \in c} \mathcal{E}(e) \qquad (1)$$

is true.

Note that the cycles form a vector space and for a finite QG only a finite number of cycles need to be examined (see Thimm & Winkler, 2006). Typically, the elements of $\mathcal{E}$ do not exceed the range $-1, \ldots, 1$.

Fig. 1 shows an example for a QG and an embedding. That equation (1) in Definition 3.1 is fulfilled is shown for two selected cycles: $(e_1, \bar{e}_2)$ and (e_1, e_5, e_3),

$$\mathbf{v}_1 - \mathbf{v}_2 = \begin{pmatrix} 0-0 \\ 1-0 \end{pmatrix}$$
$$\stackrel{!}{=} \mathcal{E}(e_1) + \mathcal{E}(\overline{e}_2) = \begin{pmatrix} 0.3-0.3 \\ 0.5+0.5 \end{pmatrix} = \begin{pmatrix} 0 \\ 1 \end{pmatrix},$$
$$\mathbf{v}_1 + \mathbf{v}_5 + \mathbf{v}_3 = \begin{pmatrix} 0+1+0 \\ 1+0+0 \end{pmatrix}$$
$$\stackrel{!}{=} \mathcal{E}(e_1) + \mathcal{E}(e_5) + \mathcal{E}(e_3) = \begin{pmatrix} 0.3+0.4+0.3 \\ 0.5+0.5+0.0 \end{pmatrix}.$$

A trivial constraint – no two atoms can occupy the same location – is expressed in the following definition.

Definition 3.2. Non-confusing embedding of a QG. An embedding $\mathcal{E}$ of a QG is called non-confusing if for all paths $p = (n, \ldots, n')$ with $(n \neq n')$ the equation

$$\sum_{e \in p'} \mathcal{E}(e) \neq \mathbf{0} \tag{2}$$

holds.

(The case $n = n'$ and $\sum_{e \in p} \mathbf{v} \neq \mathbf{0}$ is covered by Definition 3.1.)

A non-confusing embedding of a QG is shown to result in the equivalent to what Delgado-Friedrichs & O'Keeffe (2003) define as a stable net or a net without collisions.

Equation (2) implies that $\mathcal{E}(e)$ is nonzero for all edges – which is true for $\mathbf{Q}^{\mathrm{L}}$ (this QG is shown in Fig. 1). Definition 3.2 is also fulfilled for $p = (e_2, e_6)$ as $\mathcal{E}(e_2) + \mathcal{E}(e_6) = (-0.1, -0.5)$.

The embedding of a simply connected net[1] is obtained by selecting a lattice (the unit cell) and assigning coordinates to a selected node. The coordinates of all other nodes are determined by the relative positions given by the embedding of the underlying QG.

Definition 3.3. Embedding of a connected net in fractional coordinates. Let

(1) $\mathbf{p} \in \mathbb{R}^D$ be the position of a designated node n in the QG (typically $0 \leq p_i < 1$), and

(2) $\mathcal{E}$ be an embedding of $\mathbf{Q}$.

The embedding $\mathcal{F}_{\mathcal{E},n,\mathbf{p}}$ of a net $\mathbf{G} = \langle \mathbf{Q}, \mathbb{Z}^D \rangle$ is a function $\mathbf{G}_N \rightarrow \mathbb{R}^D$. It is defined as

$$\mathcal{F}_{\mathcal{E},n,\mathbf{p}}(n(\mathbf{x})) = \mathbf{x} + \mathbf{p} \tag{3}$$

if $n(\mathbf{x})$ is generated from n and (inductively)

$$\mathcal{F}_{\mathcal{E},n,\mathbf{p}}(n''(\mathbf{x} + \mathbf{v})) = \mathcal{F}_{\mathcal{E},n,\mathbf{p}}(n'(\mathbf{x})) + \mathcal{E}(e) \tag{4}$$

if $e = (n' \stackrel{\mathbf{v}}{\rightarrow} n'') \in \mathbf{Q}_E$.

Fig. 2 shows the embedding $\mathcal{F}_{\mathcal{E},n_4,(0.3,0.25)}$ of $\langle \mathbf{Q}^{\mathrm{L}}, \mathbb{Z}^3 \rangle$. For instance, equation (3) places the nodes $n_4(0,0)$ and $n_4(1,1)$ at $(0.3, 0.25)^T$ and $(1.3, 1.25)^T$, respectively. As only n_3 is connected to n_4, only the positions of nodes $n_3(\mathbf{x})$ can be determined immediately. For example,

$$\begin{aligned} \mathcal{F}(n_3(0,0)) &= \mathcal{F}(n_4(0,0)) + \mathcal{E}(\overline{e}_6) \\ &= (0.3, 0.25)^T - (-0.5, 0.0)^T \\ &= (0.8, 0.25)^T \text{ or} \\ \mathcal{F}(n_3(1,2)) &= (1.8, 2.25)^T. \end{aligned}$$

The knowledge of the positions of all nodes $n_3(\mathbf{x})$ allows one to determine the fractional coordinates of the remaining nodes:

$$\begin{aligned} \mathcal{F}(n_1(1,1)) &= \mathcal{F}\big(n_1((1,2)^T - \mathbf{v}_1)\big) \\ &= \mathcal{F}(n_3(1,2)) - (0.3, 0.5)^T \\ &= (1.5, 1.75)^T \text{ or} \\ \mathcal{F}(n_2(1,1)) &= \mathcal{F}(n_2(0,1) + \mathbf{v}_5) \\ &= \mathcal{F}(n_3(0,1)) + (0.4, 0.5)^T \\ &= (0.8, 1.25)^T + (0.4, 0.5)^T \\ &= (1.2, 1.75)^T. \end{aligned}$$

Proposition 3.4. The embedding of a connected net is non-confusing (that is, no two nodes are co-located) if and only if the underlying QG is non-confusing.

Proof. As the net is connected, the QG is also connected. Assume that the QG is confusing: there exists a path that confuses two nodes. This path is mapped for all embeddings of the net onto a path with distinct, co-located nodes. *Vice versa*, assume two nodes in the net's embedding are co-located. As the net is connected, a path connects them. This path corresponds to a path in the QG and it can be shown that this path violates Definition 3.1 or 3.2.

A few remarks are due:

(1) For QGs defining 'parallel', disconnected nets [such as that of marcasite; see Thimm (2008) for a definition] with a multiplicity M larger than one or those defined by disconnected QGs, several nodes need to be positioned. The pair $\mathbf{p}, n$ has to be replaced by the set $\{\mathbf{p}^{(n_{i,m})} \in \mathbb{R}^D | 1 \leq m \leq M$ of sub-QG $i\}$. For example, the marcasite net would require two pairs of nodes and positions.

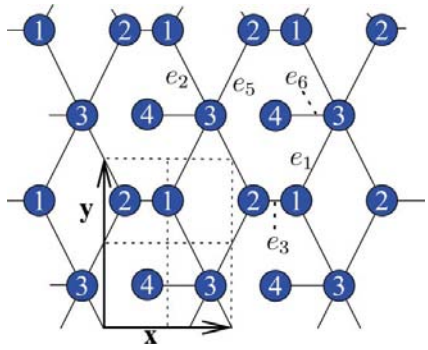

Figure 2
The embedding $\mathcal{F}_{\mathcal{E},n_4,(0.3,0.25)}$ of $\langle \mathbf{Q}^{\mathrm{L}}, \mathbb{Z}^3 \rangle$.

[1] Equivalent to a net in Delgado-Friedrichs & O'Keeffe (2003), where $\mathcal{E}$ plays the role of the *placement* function.

(2) Disconnected nets with a connected QG and a multiplicity of one (*e.g.* layered nets like those of graphite or serpentine) can be represented using Definition 3.3.

(3) The definition of a non-confusing embedding of a QG can be extended to disconnected QGs or QGs with a multiplicity higher than one if the relative positions of the sub-nets are taken into account. For all pairs of nodes $n' \neq n''$ with

(*a*) $n_{i,m}$ in the same subgraph as n' and assigned to the vector $\mathbf{p}^{n_{i,m}}$,

(*b*) $n_{j,n}$ in the same subgraph as n'' and assigned to the vector $\mathbf{p}^{n_{j,n}}$,

(*c*) p' some path between $n_{i,m}$ and n', and

(*d*) p'' some path between $n_{i,m}$ and n'',

the equation $\mathbf{p}^{(n_{i,m})} + \sum_{e\in p'} \mathcal{E}(e) \neq \mathbf{p}^{(n_{j,n})} + \sum_{e\in p''} \mathcal{E}(e)$ must hold.

4. Symmetries of embeddings

It was shown in Thimm & Winkler (2006) and Thimm (2008) how the automorphisms of a QG allow one to determine the (super-)space group for the symmetries of all possible embeddings of the net defined by the QG. In other words, the topology of a net defines the maximal symmetry an embedding – and therefore a structure – can have. This section addresses the relationship between an embedding and this maximal symmetry. It will be shown that the symmetry of an embedded net is effectively determined by the embedding of the QG.

Each QG possesses a set of automorphisms (maps of edges and nodes) that are consistent with automorphisms of the net. For each QG automorphism, a rotational component and intrinsic translations of the symmetry elements of a suitable embedding of the net can be determined (Thimm & Winkler, 2006). The embedding of the net (the fractional coordinates $\mathbf{p}$ assigned to node n) determines essentially the setting of the net. The automorphisms φ_i of the QG are identified with the elements of the space group $g_i \in \mathcal{G}$ of the embedding of the net. The elements g_i may, depending on the context, operate on

(1) the nodes and edges of the QG, or

(2) on the positions of nodes in an embedding of a net.

In the latter case, g is a Seitz symbol $(\mathbf{W}, \mathbf{w})$ which operates on fractional coordinates $\mathbf{p}_i$ of nodes n_i with $\mathbf{p}_j = \lfloor \mathbf{W}\cdot\mathbf{p}_i + \mathbf{w}\rfloor$, $g(n_i) = n_j$, and $\lfloor\mathbf{v}\rfloor$ adds a suitable integer vector to $\mathbf{v}$ such that the result is a vector in $[0, 1)^D$. Note that vectors $\mathbf{w}$ are sums of intrinsic translations $\mathbf{w}^{(i)}$ (determined by the QG automorphism) and locational translations $\mathbf{w}^{(l)}$ (defined by the setting).

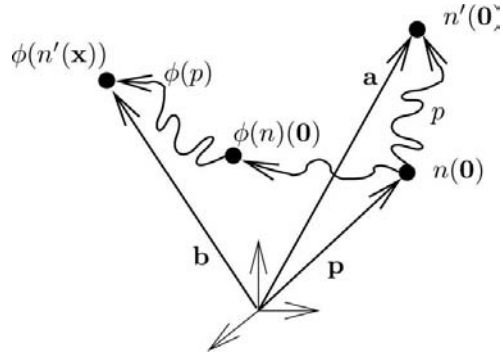

Figure 3
The mapping of the nodes and paths under φ.

It follows that if $(\mathbf{W}, \mathbf{w})$ describes a symmetry of an embedded net, then $(\mathbf{W}, \mathbf{w})$ is associated to some automorphism of the QG. However, the inverse statement may or may not be true. The following elucidates this discrepancy by first defining an embedding of a QG, then defining an embedding of a net and finally proposing when a net possesses a certain symmetry.

Definition 4.1. Compliance of a QG embedding with an automorphism. A (consistent) embedding complies with a set Φ of automorphisms φ_i if for the matrices $\mathbf{W}_i$ associated with each φ_i the equation

$$\mathcal{E}(\varphi_i(e)) = \mathbf{W}_i \cdot \mathcal{E}(e) \tag{5}$$

holds for all $e \in \mathbf{Q}_E$.

Proposition 4.2. If a (consistent) embedding $\mathcal{E}$ of a QG $\mathbf{Q}$ is compliant with an automorphism φ and $\mathbf{G} = \langle \mathbf{Q}, \mathbb{Z}^D\rangle$ is connected, then there exists a vector $\mathbf{w} \in \mathbb{R}^D$ such that for an arbitrary choice of n and $\mathbf{p}$ the embedding $\mathcal{F}_{\mathcal{E},n,\mathbf{p}}$ has a symmetry with Seitz symbol $(\mathbf{W}, \mathbf{w})$.

Proof. Let $n'(\mathbf{x})$ be an arbitrary node in the net. As the net is connected, there exists a path p in the QG, which, if mapped onto the net, has the first node $n(\mathbf{0})$ and the last node $n'(\mathbf{x})$. As $\mathbf{Q}$ is compliant with φ, it follows that

$$\sum_{e\in p} \mathcal{E}(\varphi(e)) = \sum_{e\in p} \mathbf{W}\cdot\mathcal{E}(e) = \mathbf{W}\cdot\sum_{e\in p}\mathcal{E}(e).$$

Choose $n \in \mathbf{Q}_N$, $\mathbf{p} \in \mathbb{R}^D$ and a path q with $\sum_{e\in q} \mathbf{v} = \mathbf{0}$ that is the image of the path connecting $n(\mathbf{0})$ and $\varphi(n(\mathbf{0}))$. (Each QG is isomorphic to a QG that has a spanning tree with all edges in this tree having zero labels.) This is possible as the automorphism φ of the QG can be understood as the image of the quotient of net automorphisms φ and the translations, which implies that the automorphism of the net can be chosen such that $\varphi(n(\mathbf{0})) = \varphi(n)(\mathbf{0})$. It follows that (see also Fig. 3)

$$\mathbf{W}\mathbf{p} + \mathbf{w}_0 = \mathbf{p} + \sum_{e\in q}\mathcal{E}(e). \tag{6}$$

As $\mathbf{Q}$ is compliant, equation (5) implies for path p that

$$\sum_{e\in p}\mathbf{W}\mathcal{E}(e) = \sum_{e\in p}\mathcal{E}(\varphi(e)) = \sum_{e\in\varphi(p)}\mathcal{E}(e). \tag{7}$$

Combining equations (6) and (7) gives

Table 1
The automorphisms of $\mathbf{Q}^{\mathrm{L}}$.

φ_n	$\mathbf{W}_i$	Node orbits	Edge orbits
φ_1	$\begin{pmatrix} 1 & 0 \\ 0 & -1 \end{pmatrix}$	$[n_1], [n_2], [n_3], [n_4]$	$[e_1, e_2], [e_3], [e_4, \bar{e}_5], [e_6]$
φ_2	$\begin{pmatrix} -1 & 0 \\ 0 & 1 \end{pmatrix}$	$[n_2, n_1], [n_3], [n_4]$	$[\bar{e}_1, \bar{e}_4], [e_2, \bar{e}_5], [e_3, \bar{e}_3], [e_6]$
φ_3	$\begin{pmatrix} -1 & 0 \\ 0 & -1 \end{pmatrix}$	$[n_1, n_2], [n_3], [n_4]$	$[\bar{e}_1, e_5], [e_2, e_4], [e_3, \bar{e}_3], [e_6]$

$$\begin{aligned} &\mathbf{W}\mathbf{p} + \mathbf{w}_0 + \sum_{e\in p} \mathbf{W}\mathcal{E}(e) \\ &\quad = \mathbf{W}\underbrace{\left(\mathbf{p} + \sum_{e\in p} \mathcal{E}(e)\right)}_{\mathbf{a}} + \mathbf{w}_0 \\ &\quad = \underbrace{\mathbf{p} + \sum_{e\in q} \mathcal{E}(e) + \sum_{e\in\varphi(p)} \mathcal{E}(e)}_{\mathbf{b}}. \end{aligned} \tag{8}$$

In equation (8) as well as Fig. 3, the vector **a** describes the position of the node $n'(\mathbf{x})$ whereas **b** describes the position of one of its images. As $n'(\mathbf{x})$ was chosen arbitrarily and $\mathbf{W}$ and $\mathbf{w}_0$ are independent of this choice, this applies to all nodes in the net.

It is left to show that $\mathbf{w} \in [0, 1)^D$ exists [such that $(\mathbf{W}, \mathbf{w})$ is a Seitz symbol]. This is shown by changing the construction above slightly: choose q' such that it connects $n(\mathbf{0})$ and $\varphi(n)(-\lfloor \mathbf{w}_0 \rfloor)$. Then, start $\varphi(p)$ at the end node of q'. Again, the end node of p and $\varphi(p)$ are isomorphic. However, in equation (8), the term $\mathbf{w}_0$ is replaced by $\mathbf{w}_0 - \lfloor \mathbf{w}_0 \rfloor$. Defining $\mathbf{w} = \mathbf{w}_0 - \lfloor \mathbf{w}_0 \rfloor$ yields the desired result.

The proof above also shows that the choice of n and $\mathbf{p}$ has no influence on whether $\mathcal{F}_{\mathcal{E},n,\mathbf{p}}(\langle \mathbf{Q}, \mathbb{Z}^D \rangle)$ possesses a given symmetry or not.

5. Permissible symmetries

The above shows that the automorphism group $\mathcal{G}^{\mathrm{QG}}$ defined by a QG is a supergroup to the automorphism group $\mathcal{G}^{\mathrm{QG},\mathcal{E}}$ of the QG constrained by an embedding of the QG. Likewise, the group $\mathcal{G}^{\mathrm{net},\mathcal{E}}/\mathcal{T}$ of a given embedding of a net (where $\mathcal{G}^{\mathrm{net},\mathcal{E}}/\mathcal{T}$ is the normal subgroup of $\mathcal{G}^{\mathrm{net},\mathcal{E}}$ with respect to the translations $\mathcal{T}$) is isomorphic to a subgroup of $\mathcal{G}^{\mathrm{QG},\mathcal{E}}$ (the lattice may be incompatible with some φ). The group and $\mathcal{G}^{\mathrm{QG},\mathcal{E}}$ are isomorphic. The following therefore focuses on the relationship between $\mathcal{G}^{\mathrm{QG}}$ and $\mathcal{G}^{\mathrm{QG},\mathcal{E}}$, that is the interaction of $\mathcal{E}$ and symmetries.

The constraint on an embedding to be consistent and compliant with a set of automorphisms-*cum*-symmetries can be used to establish a linear set of equations constraining $\mathcal{E}$. The relationship between the constraints and the symmetry of an embedding is rather strong. If sets Φ_1 and Φ_2 of automorphisms correspond to set $\mathcal{G}_1$ and $\mathcal{G}_2$ of symmetry operations, and set $\mathcal{G}_2$ is generated from $\mathcal{G}_1$, then the constraints arising from Φ_1 and Φ_2 on the embedding of a QG are identical. Turning this statement around, if a set of constraints for the set of automorphisms Φ_1 and $\Phi_1 \cup \Phi_2$ have the same degrees of freedom, then the symmetry elements of $\mathcal{G}_2$ are generated by $\mathcal{G}_1$.

6. Properties of selected nets and structures

In this section, two two-dimensional nets (one built from lozenges and hexagons, represented by the QG $\mathbf{Q}^{\mathrm{L}}$, and a hexagon net described by $\mathbf{Q}^{\mathrm{H}}$) and several nets derived from known structures are used to exemplify some of the observations and conclusions that can be drawn. Only observations that are impossible using group theory are highlighted.

6.1. The embedding of $\mathbf{Q}^{\mathrm{L}}$

The example in §2 illustrated that for a given QG the demand for an embedding to be non-confusing may eliminate symmetries. Such cases can be recognized by examining the linear set resulting from Definitions 3.1 and 3.2. The QG shown in Fig. 2 represents a case where certain symmetries result in a confusing embedding: due to the edge between nodes n_3 and n_4, an embedding of the net has either a reflection symmetry parallel to the x axis or the y axis, but not both. This can be shown formally. $\mathbf{Q}^{\mathrm{L}}$ has four automorphisms: the identity, one which corresponds to a twofold rotation and two others which correspond to perpendicular mirror planes. Table 1 shows the latter three symmetries along with node and edge orbits.

Automorphism φ_1 corresponds to a reflection perpendicular to the x axis. Equation (5) and orbit $[e_6]$ constrain the embedding of e_6 [$(x_i, y_i)^T$ denotes the value of $\mathcal{E}(e_i)$]:

$$\mathcal{E}(\varphi_1(e_6)) = \mathcal{E}(e_6) = \begin{pmatrix} x_6 \\ y_6 \end{pmatrix},$$
$$\mathbf{W}_1 \cdot \mathcal{E}(e_6) = \begin{pmatrix} 1 & 0 \\ 0 & -1 \end{pmatrix} \cdot \begin{pmatrix} x_6 \\ y_6 \end{pmatrix} = \begin{pmatrix} x_6 \\ -y_6 \end{pmatrix},$$

which implies that $y_6 = -y_6 = 0$. The automorphism φ_2, which corresponds to a reflection perpendicular to the y axis, further constrains $\mathcal{E}(e_6)$ *via* orbit $[e_6]$: $x_6 = -x_6 = 0$. It follows that $\mathcal{E}(e_6) = \mathbf{0}$ if both symmetries are enforced. An embedding realizing the two automorphisms is consequently confusing. In other words, the QG $\mathbf{Q}^{\mathrm{L}}$ and the resulting net can only be embedded such that at most one of the two reflections is realized [or the translational symmetry is reduced, which is equivalent to increasing the size of the QG; see Schumacher (1994)].

The rotation can be completely excluded: from orbit $[e_6]$ for φ_3 it follows directly that $x_6 = 0 = y_6$. It can be concluded that an embedding $\mathcal{F}_{\mathcal{E},n,\mathbf{p}}(\langle \mathbf{Q}^{\mathrm{L}}, \mathbb{Z}^2 \rangle)$ can only have the symmetry of plane group pm or $p1$.

A further examination of the constraints resulting from φ_1 and the consistency of the QG shows that these only correspond to nine independent constraints. This allows one to choose freely three variables. The embeddings compliant with φ_1 can be described with ($s, t, u, v, w \in \mathbb{R}$)

$$(\mathcal{E}(e_1), \ldots, \mathcal{E}(e_6)) = \begin{pmatrix} s & s & 1-2s & -s & s & 0 \\ 1-t & -t & 0 & 1-t & t & u \end{pmatrix}$$

and those by φ_2 with

$$(\mathcal{E}(e_1), \ldots, \mathcal{E}(e_6)) = \begin{pmatrix} 1-v-s & 1-v-s & v & -s & s & w \\ \frac{1}{2} & -\frac{1}{2} & 0 & \frac{1}{2} & \frac{1}{2} & 0 \end{pmatrix}.$$

However, both can be fulfilled for appropriate choices for the free variables ($u = w = 0$, $v = 1 - 2s$, $t = \frac{1}{2}$) if the conflict for e_6 is set aside. For this choice of variable, the constraints for φ_3 are fulfilled and the embedding is

$$(\mathcal{E}(e_1), \ldots, \mathcal{E}(e_6)) = \begin{pmatrix} s & s & 1-2s & -s & s & 0 \\ \frac{1}{2} & -\frac{1}{2} & 0 & \frac{1}{2} & \frac{1}{2} & 0 \end{pmatrix}.$$

This embedding, though conflicting, does not fully determine all relative node positions. In general, an embedding may be confusing, not fully constrained, or both.

6.2. The hexagon net Q^H

Fig. 4 shows $\mathbf{Q}^{\mathrm{H}}$ and an arbitrary embedding of its net. An embedding with maximal symmetry would result in the hexagon net (similar to a layer of the graphite structure). However, despite being arbitrary, Fig. 4 evokes the presence of twofold rotations at positions indicated by the lentil-like shapes in the lower right of the figure. The following demonstrates that all embeddings of $\mathbf{Q}^{\mathrm{H}}$ have this symmetry.

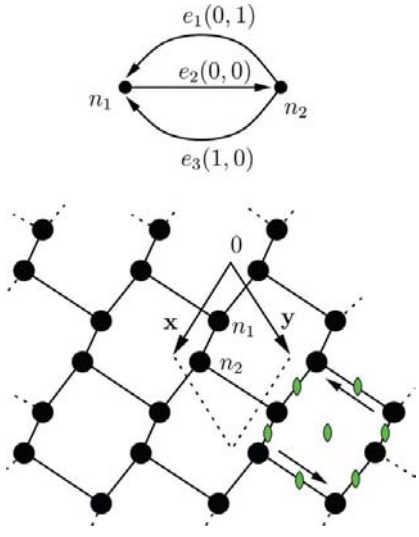

Figure 4
The QG $\mathbf{Q}^{\mathrm{H}}$ and an arbitrary embedding of its net.

The automorphism φ_1 corresponds to a twofold rotation with

$$\mathbf{W}_1 = \begin{pmatrix} -1 & 0 \\ 0 & -1 \end{pmatrix}$$

and has three edge orbits: $[e_1, \overline{e}_1]$, $[e_2, \overline{e}_2]$ and $[e_3, \overline{e}_3]$. These orbits result in rather similar constraints ($1 \le i \le 3$):

$$\mathcal{E}(\varphi(e_i)) = \mathbf{W}_1 \cdot \mathcal{E}(\overline{e}_i) \Leftrightarrow \begin{pmatrix} -x_i \\ -y_i \end{pmatrix} = \begin{pmatrix} -x_i \\ -y_i \end{pmatrix}$$
$$\mathcal{E}(\varphi(\overline{e}_i)) = \mathbf{W}_1 \cdot \mathcal{E}(e_i) \Leftrightarrow \begin{pmatrix} x_i \\ y_i \end{pmatrix} = \begin{pmatrix} x_i \\ y_i \end{pmatrix}.$$

These constraints are, however, true for any $\mathcal{E}$, and therefore a twofold rotation is compatible with all two-dimensional lattices. It can be concluded that all embeddings of $\mathbf{Q}^{\mathrm{H}}$ have a twofold rotational symmetry.

On the other hand, Fig. 4 shows that threefold rotations are not necessarily present in all embeddings of $\mathbf{Q}^{\mathrm{H}}$ even if corresponding QG automorphisms exist. Automorphism φ_2 generates the edge orbit $[e_1, \overline{e}_2, e_3]$ and is associated with the matrix

$$\mathbf{W}_2 = \begin{pmatrix} -1 & -1 \\ 1 & 0 \end{pmatrix}.$$

Equation (5) results in

$$\mathcal{E}(\varphi(e_1)) = \mathbf{W}_2 \cdot \mathcal{E}(e_1) \Leftrightarrow \begin{pmatrix} -x_2 \\ -y_2 \end{pmatrix} = \mathbf{W}_2 \cdot \begin{pmatrix} x_i \\ y_i \end{pmatrix} = \begin{pmatrix} -x_1 - y_1 \\ x_1 \end{pmatrix}$$
$$\mathcal{E}(\varphi(e_2)) = \mathbf{W}_2 \cdot \mathcal{E}(e_2) \Leftrightarrow \begin{pmatrix} -x_3 \\ -y_3 \end{pmatrix} = \mathbf{W}_2 \cdot \begin{pmatrix} x_2 \\ y_2 \end{pmatrix} = \begin{pmatrix} -x_2 - y_2 \\ x_2 \end{pmatrix}$$
$$\mathcal{E}(\varphi(e_3)) = \mathbf{W}_2 \cdot \mathcal{E}(e_3) \Leftrightarrow \begin{pmatrix} x_i \\ y_i \end{pmatrix} = \mathbf{W}_2 \cdot \begin{pmatrix} x_3 \\ y_3 \end{pmatrix} = \begin{pmatrix} -x_3 - y_3 \\ x_3 \end{pmatrix}.$$

Equation (1) applied to cycles (e_1, e_2) and (e_2, e_3) implies that

$$\begin{pmatrix} x_1 + x_2 \\ y_1 + y_2 \end{pmatrix} = \begin{pmatrix} 0 \\ 1 \end{pmatrix} \text{ and } \begin{pmatrix} x_2 + x_3 \\ y_2 + y_3 \end{pmatrix} = \begin{pmatrix} 1 \\ 0 \end{pmatrix}.$$

These equations have a unique solution:

$$\mathcal{E}(e_1) = \begin{pmatrix} -\frac{1}{3} \\ \frac{2}{3} \end{pmatrix}, \quad \mathcal{E}(e_2) = \begin{pmatrix} -\frac{1}{3} \\ \frac{1}{3} \end{pmatrix}, \quad \mathcal{E}(e_3) = \begin{pmatrix} \frac{2}{3} \\ -\frac{1}{3} \end{pmatrix}. \tag{9}$$

$\mathcal{F}_{\mathcal{E},n_1,(0,0)}$ positions the nodes on the centres of the threefold rotations in a suitable unit cell and is equivalent to the standard setting of the two-dimensional plane group $p3$ [as given in Hahn (1992)]. Such an embedding already possesses the symmetry of *p6mm*. This can be verified by a comparison of the symmetries of *p6mm* with $\mathcal{F}$ or the argument that the

embedding $\mathcal{E}$ is fully constrained and the knowledge that the hexagon net has this very symmetry.

The third and last automorphism of $\mathbf{Q}^{\rm H}$ examined here has two edge orbits $[e_3]$ and $[e_1, \bar{e}_2]$ and corresponds to a reflection with

$$\mathbf{W}_3 = \begin{pmatrix} 1 & 0 \\ -1 & -1 \end{pmatrix}.$$

Equation (5) results in $y_3 = -\frac{1}{2}x_3$ for the first orbit and $x_2 = -x_1$ and $y_1 = x_2 + y_2$ for the second orbit (and other redundant constraints). These constraints, together with the consistency of the QG, result in the embedding

$$\mathcal{E}(e_1) = \begin{pmatrix} x-1 \\ 1-\frac{1}{2}x \end{pmatrix}, \quad \mathcal{E}(e_2) = \begin{pmatrix} 1-x \\ \frac{1}{2}x \end{pmatrix},$$
$$\mathcal{E}(e_3) = \begin{pmatrix} x \\ -\frac{1}{2}x \end{pmatrix} \quad \text{with } x \in \mathbb{R}. \tag{10}$$

For x = 2/3 the embeddings described by equations (9) and (10) are identical. However, if x is not further constrained, the relative positions of the nodes are not definite. For x = 0.55 and a compatible unit cell, the embedding $\mathcal{F}_{\mathcal{E},n_1,(0.450,0.225)}$ results in Fig. 5. For increasing x, the nodes are displaced as indicated by the arrows in Fig. 5 until for x = 2/3 the perfect hexagon net is achieved.

In summary, embeddings of the hexagon net with a maximal translational symmetry (that is two nodes per unit cell) always have a twofold rotational symmetry. Whether or not a threefold rotation or one or more reflections are observable for the embedding of the net depends on the node positions as well as the lattice. If the constraints for a threefold rotational symmetry are fulfilled, then this is also true for the reflections; the embedding can have the symmetry *p6mm* but *p*6 or *p*3 are forbidden.

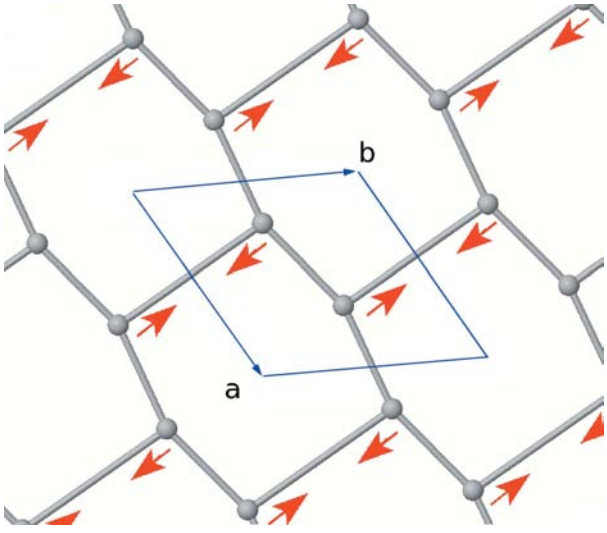

Figure 5
An embedding of $\mathbf{Q}^{\rm H}$ for $\mathbf{W}_3$, x = 0.55 and $\mathcal{F}_{\mathcal{E},n_1,(0.450,0.225)}$. Vectors **a** and **b** indicate a valid choice for the coordinate system for the embedding.

6.3. Halite

Halite (NaCl) crystallizes in space group $Fm\bar{3}m$ (Putnis, 1992). In a conventional setting, Na atoms are at the fractional coordinates (0, 0, 0) and Cl atoms are at $(0, \frac{1}{2}, 0)$ (Wenk & Bulakh, 2004). For the purpose of determining which symmetries require particular relative positions of the atoms and which are independent of these, the QG $\mathbf{Q}^{\rm halite}$ was determined for a primitive cell containing one formula unit:

$$e_1 = \mathrm{Cl} \xrightarrow{(1,0,0)} \mathrm{Na}, \quad e_2 = \mathrm{Cl} \xrightarrow{(0,1,0)} \mathrm{Na},$$
$$e_3 = \mathrm{Cl} \xrightarrow{(0,0,1)} \mathrm{Na}, \quad e_4 = \mathrm{Cl} \xrightarrow{(1,1,0)} \mathrm{Na},$$
$$e_5 = \mathrm{Cl} \xrightarrow{(1,0,1)} \mathrm{Na}, \quad e_6 = \mathrm{Cl} \xrightarrow{(0,1,1)} \mathrm{Na}.$$

This QG possesses automorphisms corresponding to all symmetries observed for the halite structure, as well as automorphisms exchanging the Na and the Cl atoms. The latter are disregarded in the following. One of the automorphisms, referred to as φ_1, corresponds to a threefold rotation with matrix

$$\mathbf{W}_1 = \begin{pmatrix} 0 & 0 & 1 \\ 1 & 0 & 0 \\ 0 & 1 & 1 \end{pmatrix}$$

and the edge orbits $[e_1, e_2, e_3,]$ and $[e_4, e_6, e_5]$. In order for the embedding of the QG to comply with this automorphism, the following has to be fulfilled $[\mathcal{E}(e_i) = \mathbf{W}\mathbf{u}_i]$:

$$\mathbf{u}_2 = \mathbf{W}_1\mathbf{u}_1, \qquad \mathbf{u}_3 = \mathbf{W}_1\mathbf{u}_2,$$
$$\mathbf{u}_1 = \mathbf{W}_1\mathbf{u}_3, \qquad \mathbf{u}_6 = \mathbf{W}_1\mathbf{u}_4,$$
$$\mathbf{u}_5 = \mathbf{W}_1\mathbf{u}_6, \qquad \mathbf{u}_4 = \mathbf{W}_1\mathbf{u}_5.$$

Furthermore, in order for the QG to be consistent,

$$\mathbf{u}_1 - \mathbf{u}_2 = (1, -1, 0)^T,$$
$$\mathbf{u}_1 - \mathbf{u}_3 = (1, 0, -1)^T,$$
$$\mathbf{u}_1 - \mathbf{u}_4 = (0, -1, 0)^T,$$
$$\mathbf{u}_1 - \mathbf{u}_5 = (0, 0, -1)^T,$$
$$\mathbf{u}_1 - \mathbf{u}_6 = (1, -1, -1)^T.$$

Solving these equations results in

$$(\mathcal{E}(e_1), \ldots, \mathcal{E}(e_6)) = \begin{pmatrix} x & x-1 & x-1 & x & x & x-1 \\ x-1 & x & x-1 & x & x-1 & x \\ x-1 & x-1 & x & x-1 & x & x \end{pmatrix},$$

with the ith column being $\mathcal{E}(e_i)$ and $x \in \mathbb{R}$. For $x = \frac{1}{2}$, the embedding $\mathcal{F}_{\mathcal{E},\mathrm{Cl},(0,0,0)}(\langle \mathbf{Q}^{\rm halite}, \mathbb{Z}^3 \rangle)$ corresponds to a setting of NaCl with Cl at the origin of a primitive cell. In order for the structure to have this symmetry, this primitive cell must have a rhombohedral or cubic shape. However, constraining the embedding to possess one threefold rotation and a cubic unit cell does not necessarily result in a cubic symmetry. This can readily be seen if one realizes that in an embedding with cubic

Table 2
Remaining degrees of freedom of an embedding of the diamond QG.

The translational symmetry is included. Rotations and reflections may have a translational component.

Automorphism	Freedom
F-centring translations	3
$\bar{1}$	3
2[100], 2[010], 2[001]	1
2[011], 2[110], 2[101]	2
m[100], *m*[010], *m*[001]	1
m[011], *m*[110], *m*[101]	2
3[111], 3[1$\bar{1}$1], 3[$\bar{1}$11], 3[$\bar{1}\bar{1}$1]	1
$\bar{3}$[111], $\bar{3}$[1$\bar{1}$1], $\bar{3}$[$\bar{1}$11], $\bar{3}$[$\bar{1}\bar{1}$1]	1
$\bar{4}$[100], $\bar{4}$[010], $\bar{4}$[001]	0
4[100], 4[010], 4[001]	0

symmetry all edges have to have the same length. Contrary to this, the lengths of the edges $|e_1| = (3x^2 - 4x + 2)^{1/2}$ and $|e_4| = (3x^2 - 2x + 1)^{1/2}$ are only equal for $x = \frac{1}{2}$.

The automorphism corresponding to an inversion has the edge orbits $[e_1, e_6]$, $[e_2, e_5]$ and $[e_3, e_4]$. This implies that $\mathbf{u}_6 = -\mathbf{u}_1$, $\mathbf{u}_5 = -\mathbf{u}_2$ and $\mathbf{u}_4 = -\mathbf{u}_3$. Combining these resolves to

$$(\mathcal{E}(e_1), \ldots, \mathcal{E}(e_6)) = \begin{pmatrix} \frac{1}{2} & -\frac{1}{2} & -\frac{1}{2} & \frac{1}{2} & \frac{1}{2} & -\frac{1}{2} \\ -\frac{1}{2} & \frac{1}{2} & -\frac{1}{2} & \frac{1}{2} & -\frac{1}{2} & \frac{1}{2} \\ -\frac{1}{2} & -\frac{1}{2} & \frac{1}{2} & -\frac{1}{2} & \frac{1}{2} & \frac{1}{2} \end{pmatrix}.$$

This fully defines the embedding. As an embedding with a cubic symmetry is known, it can be concluded that any structure with the halite topology, an inversion symmetry and a cubic (rhombohedral, orthogonal, monoclinic) unit cell has forcibly a cubic (rhombohedral, orthogonal, monoclinic) symmetry. Without constraints from symmetries, the embedding has three degrees of freedom. A variation of one of these is equivalent to displacing the Na lattice relative to the Cl lattice along an axis (causing bonds to have distinct lengths).

6.4. Diamond

The diamond structure has in the standard setting the symmetry of space group $Fd\bar{3}m$. Here we take the structure data from Downs & Hall-Wallace (2003). The corresponding QG has eight nodes, 16 edges and 192 automorphisms. The ensemble of all automorphisms constrains $\mathcal{E}$ such that all edge vectors have the form $(\pm\frac{1}{4}, \pm\frac{1}{4}, \pm\frac{1}{4})$ and $\mathcal{F}_{\mathcal{E},\mathrm{C}_1,(0,0,0)}$ places the C atoms at the expected locations. It may be worth noting that already the consistency of the QG and the translational symmetries corresponding to centring of the cell constrain $\mathcal{E}$ in a way that only three degrees of freedom are left. This is the same number as if the QG were created from a primitive cell and its embedding were not constrained by any symmetry. As with the hexagon net, the automorphisms corresponding to inversions do not constrain $\mathcal{E}$, but other automorphisms do. Table 2 shows the remaining degrees of freedom of an embedding if, besides the translational symmetries, the automorphisms which correspond to the given symmetries of the point group are imposed on the structure. Note that several symmetry elements of the space group (with distinct translational components) may correspond to one of these symmetries. From the fact that the fourfold rotations and the fourfold rotoinversion leave no degree of freedom, it can be concluded that a structure with the diamond topology and fourfold rotation or rotoinversion has a tetragonal ($I4_1/amd$) or cubic symmetry ($Fd\bar{3}m$), depending only on the shape of the unit cell.

Table 2 permits the conclusion that, with the exception of $\bar{1}$, all symmetries constrain the embedding. Thus, for any embedding respecting the translational symmetry of an *F*-centred structure, the minimal symmetry is $F\bar{1}$. Compared to this, the fourfold rotation and rotoinversions fully determine the embedding – the symmetry of the structure depends solely on the cell parameters. If the cell is cubic, the structure has the symmetry of $Fd\bar{3}m$. This is surprising if only group theory is considered: threefold rotations are not generated by $\{\bar{1}, 4\}$ or $\{\bar{1}, \bar{4}\}$.

6.5. Pyrite

Pyrite (FeS_2) and quartz (see §6.6) were selected as examples because the automorphisms of their QGs do not fully constrain embeddings and they have moderate structural complexity. Pyrite crystallizes in the cubic space group $Pa\bar{3}$. Its structure possesses – as expected of a structure in $Pa\bar{3}$ – 24 automorphisms. These correspond to the symmetry elements of $Pa\bar{3}$. The structure is shown in Fig. 6 and the associated QG is shown in Fig. 7.

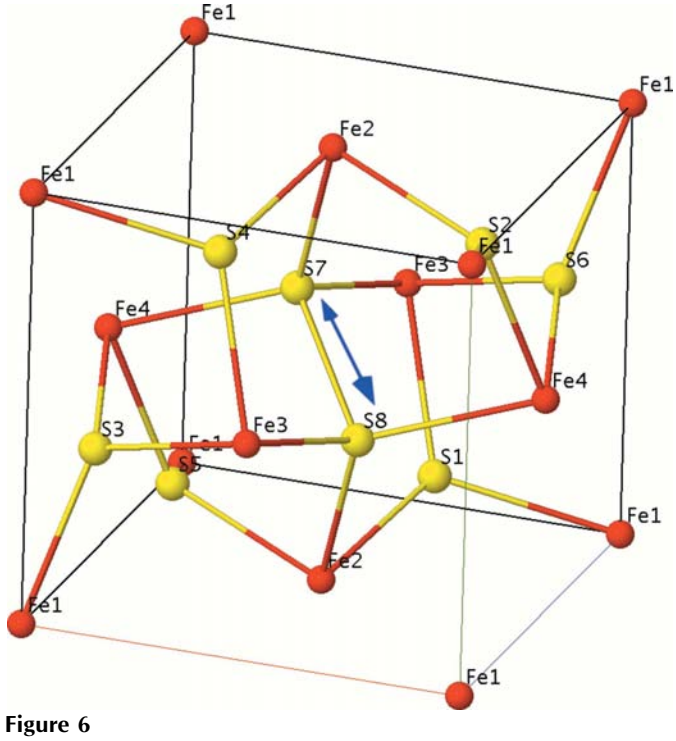

Figure 6
The structure of pyrite (Downs & Hall-Wallace, 2003).

The automorphism corresponding to the inversion is examined first. This automorphism maps all Fe nodes onto themselves, but exchanges the S node as shown in Table 3.

The Fe—S edges are all in orbits with two edges each, whereas the S—S edges are inversely mapped onto themselves. The Fe—S edge orbits form pairs which if combined accordingly result in cycles (for example, the orbits $[e_1, e_4]$ and $[e_{13}, e_{15}]$). Equation (1) implies that

$$\mathbf{u}_1 - \mathbf{u}_4 + \mathbf{u}_{15} - \mathbf{u}_{13} = \begin{pmatrix} 1 \\ 1 \\ 0 \end{pmatrix},$$

equation (5) results in $-\mathbf{u}_1 = \mathbf{u}_4$ and $-\mathbf{u}_{13} = \mathbf{u}_{15}$, and finally

$$\mathbf{u}_1 - \mathbf{u}_{13} = \begin{pmatrix} \frac{1}{2} \\ \frac{1}{2} \\ 0 \end{pmatrix}.$$

This vector relatively positions the nodes in classes Fe_1 and Fe_3 in net embeddings where they are connected to the same representative of an S_1 node. Similarly, for other pairs of Fe nodes connected to the same S node, this distance evaluates to a vector that is a permutation of $(0, \pm\frac{1}{2}, \pm\frac{1}{2})$. In other words, Fe nodes that are linked to a common S node are situated on lines that are perpendicular to one axis and at 45 or 135° to the other axes, and are at a distance equivalent to half of the diagonal of a face of the unit cell. Consequently, if the net is embedded using $\mathcal{F}_{\mathcal{E},\mathrm{Fe}_1,(0,0,0)}$ for an $\mathcal{E}$ that fulfils the constraints rising from an inversion symmetry, the Fe nodes are at the positions observed for the pyrite structure. However, only 72 independent constraints arise from the consistency of $\mathcal{E}$ and the inversion as compared to the 84 that would be required to determine the embedding completely. This leaves 12 degrees of freedom to the structure.

Compared to this, if the embedding is only constrained by a twofold screw axis, a glide plane, a single threefold rotation or a $\overline{3}$ rotoinversion, then 17, 16, 11 and 4 degrees of freedom, respectively, remain. If the structure is constrained by all symmetries, only one degree of freedom remains. Thus, the embeddings compliant with a maximal symmetry can be understood as a function $\mathcal{E}_p$ with $p \in \mathbb{R}$ representing this remaining degree of freedom. For instance, the embedding of e_1 can be expressed as

$$\mathcal{E}_p(e_1) = \begin{pmatrix} -p \\ \frac{1}{2} + p \\ -\frac{1}{2} - p \end{pmatrix}.$$

This can be carried on to the embedding $\mathcal{F}_{\mathcal{E}_p,\mathrm{Fe}_1,(0,0,0)}$. Notably, for $p = -0.3851$, which is tantamount to $\mathcal{E}(e_1) = (0.3851, 0.1149, -0.1149)$ or the position of S_1, the embedding is equivalent to the structure found in Downs & Hall-Wallace (2003). If the unit cell is chosen as in the latter structure (possessing a cubic cell with a = 5.4166 Å), the length of the Fe—S bonds is $a(3p^2 + 2p + \frac{1}{2})^{1/2}$ = 2.264 Å, whereas the S—S bonds have length $(3)^{1/2}a(2p + 1)$ = 2.156 Å (for $p \geq -\frac{1}{2}$).

The variation of p is equivalent to displacing the S atoms along straight lines parallel to the body diagonals (Wyckoff position 8*c*). The arrow in the centre of Fig. 6 indicates such a displacement (see also the supplementary video provided online[2]). These displacements stretch the S—S edge and are symmetric around the centre of the bond. A comparison with the analysis of vibrations in pyrite-type structures by Lutz *et al.* (1992) shows that two vibrational modes (A_g and $F_g(1)$) are dominantly S—S bond-stretching modes. These two modes are associated with the highest phonon energies observed for this structure type.

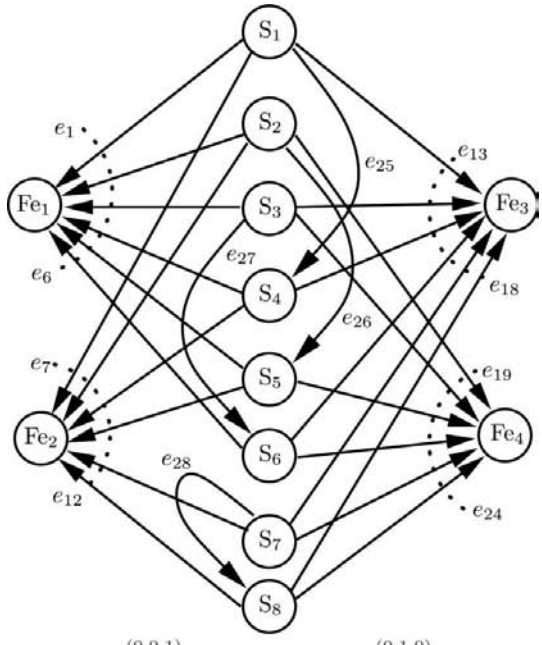

$e_1 = S_1 \xrightarrow{(0,0,1)} Fe_1$ $e_2 = S_2 \xrightarrow{(0,1,0)} Fe_1$
$e_3 = S_3 \xrightarrow{(1,0,0)} Fe_1$ $e_4 = S_4 \xrightarrow{(1,1,0)} Fe_1$
$e_5 = S_5 \xrightarrow{(1,0,1)} Fe_1$ $e_6 = S_6 \xrightarrow{(0,1,1)} Fe_1$
$e_7 = S_1 \xrightarrow{(0,0,0)} Fe_2$ $e_8 = S_2 \xrightarrow{(0,1,0)} Fe_2$
$e_9 = S_4 \xrightarrow{(0,1,0)} Fe_2$ $e_{10} = S_5 \xrightarrow{(0,0,0)} Fe_2$
$e_{11} = S_7 \xrightarrow{(0,1,0)} Fe_2$ $e_{12} = S_8 \xrightarrow{(0,0,0)} Fe_2$
$e_{13} = S_1 \xrightarrow{(0,0,1)} Fe_3$ $e_{14} = S_3 \xrightarrow{(0,0,0)} Fe_3$
$e_{15} = S_4 \xrightarrow{(0,0,0)} Fe_3$ $e_{16} = S_6 \xrightarrow{(0,0,1)} Fe_3$
$e_{17} = S_7 \xrightarrow{(0,0,1)} Fe_3$ $e_{18} = S_8 \xrightarrow{(0,0,0)} Fe_3$
$e_{19} = S_2 \xrightarrow{(0,0,0)} Fe_4$ $e_{20} = S_3 \xrightarrow{(1,0,0)} Fe_4$
$e_{21} = S_5 \xrightarrow{(1,0,0)} Fe_4$ $e_{22} = S_6 \xrightarrow{(0,0,0)} Fe_4$
$e_{23} = S_7 \xrightarrow{(1,0,0)} Fe_4$ $e_{24} = S_8 \xrightarrow{(0,0,0)} Fe_4$
$e_{25} = S_1 \xrightarrow{(0,-1,1)} S_4$ $e_{26} = S_2 \xrightarrow{(-1,1,0)} S_5$
$e_{27} = S_3 \xrightarrow{(1,0,-1)} S_6$ $e_{28} = S_7 \xrightarrow{(0,0,0)} S_8$

Figure 7
The QG of pyrite.

[2] Supplementary videos for this paper are available from the IUCr electronic archives (reference EO5001). Services for accessing these archives are described at the back of the journal.

Table 3
Selected automorphisms of the pyrite QG.

W	Symmetry	Node orbits	Edge orbits
$\begin{pmatrix} -1 & 0 & 0 \\ 0 & -1 & 0 \\ 0 & 0 & -1 \end{pmatrix}$	$\bar{1}$	$[Fe_1]$, $[Fe_2]$, $[Fe_3]$, $[Fe_4]$, $[S_4, S_1]$, $[S_5, S_2]$, $[S_6, S_3]$, $[S_7, S_8]$	$[e_1, e_8]$, $[e_2, e_7]$, $[e_3, e_{11}]$, $[e_4, e_{10}]$, $[e_5, e_9]$, $[e_6, e_{12}]$, $[e_{13}, e_{19}]$, $[e_{14}, e_{23}]$, $[e_{15}, e_{21}]$, $[e_{16}, e_{24}]$, $[e_{17}, e_{20}]$, $[e_{18}, e_{22}]$, $[e_{25}, e_{26}]$, $[e_{27}, e_{28}]$
$\begin{pmatrix} -1 & 0 & 0 \\ 0 & -1 & 0 \\ 0 & 0 & 1 \end{pmatrix}$	2_1	$[Fe_1, Fe_2]$, $[Fe_3, Fe_4]$, $[S_2, S_1]$, $[S_4, S_5]$, $[S_6, S_8]$, $[S_7, S_3]$	$[e_1, e_4]$, $[e_2, e_5]$, $[e_3, e_6]$, $[e_7, e_9]$, $[e_8, e_{10}]$, $[e_{11}, e_{12}]$, $[e_{13}, e_{15}]$, $[e_{14}, e_{16}]$, $[e_{17}, e_{18}]$, $[e_{19}, e_{21}]$, $[e_{20}, e_{22}]$, $[e_{23}, e_{24}]$, $[\bar{e}_{25}, e_{25}]$, $[\bar{e}_{26}, e_{26}]$, $[\bar{e}_{27}, e_{27}]$, $[\bar{e}_{28}, e_{28}]$
$\begin{pmatrix} 0 & 0 & 1 \\ 1 & 0 & 0 \\ 0 & 1 & 0 \end{pmatrix}$	3^-	$[Fe_1]$, $[Fe_4, Fe_2, Fe_3]$, $[S_1, S_3, S_2]$, $[S_4, S_6, S_5]$, $[S_7]$, $[S_8]$	$[e_1, e_3, e_2]$, $[e_4, e_6, e_5]$, $[e_7, e_{14}, e_{19}]$, $[e_8, e_{13}, e_{20}]$, $[e_9, e_{16}, e_{21}]$, $[e_{10}, e_{15}, e_{22}]$, $[e_{11}, e_{17}, e_{23}]$, $[e_{12}, e_{18}, e_{24}]$, $[e_{25}, e_{27}, e_{26}]$, $[e_{28}]$
$\begin{pmatrix} 0 & -1 & 0 \\ 0 & 0 & -1 \\ -1 & 0 & 0 \end{pmatrix}$	$\bar{3}^+$	$[Fe_1]$, $[Fe_4, Fe_3, Fe_2]$, $[S_1, S_5, S_3, S_4, S_2, S_6]$, $[S_8, S_7]$	$[e_1, e_5, e_3, e_4, e_2, e_6]$, $[e_7, e_{21}, e_{14}, e_9, e_{19}, e_{16}]$, $[e_8, e_{22}, e_{13}, e_{10}, e_{20}, e_{15}]$, $[e_{11}, e_{24}, e_{17}, e_{12}, e_{23}, e_{18}]$, $[\bar{e}_{25}, e_{26}, \bar{e}_{27}, e_{25}, \bar{e}_{26}, e_{27}]$, $[\bar{e}_{28}, e_{28}]$

6.6. Quartz

Among the enantiomorphic phases of quartz (SiO_2), only the phases with symmetries $P6_222$ and $P3_121$ are considered here. The QG in Fig. 8 was obtained from the high-temperature phase [structural data are taken from Downs & Hall-Wallace (2003), attributed to Kihara (1990) for T = 854 K]. An analysis of the QG's automorphism shows that embeddings constrained by all automorphisms corresponding to space groups $P6_222$ and $P3_121$ have one and four degrees of freedom, respectively.

If the constraints equivalent to all automorphisms are satisfied, the embeddings of the edges are of the form

$$\begin{aligned}
\mathcal{E}(e_1) &= \left(\tfrac{1}{2}p - \tfrac{1}{4},\ -\tfrac{1}{2}p - \tfrac{1}{4},\ \tfrac{1}{6}\right)\\
\mathcal{E}(e_2) &= \left(\tfrac{1}{2}p + \tfrac{1}{4},\ -\tfrac{1}{2}p + \tfrac{1}{4},\ -\tfrac{1}{6}\right)\\
\mathcal{E}(e_3) &= \left(-\tfrac{1}{2}p + \tfrac{1}{4},\ \tfrac{1}{2}p + \tfrac{1}{4},\ \tfrac{1}{6}\right)\\
\mathcal{E}(e_4) &= \left(-\tfrac{1}{2}p - \tfrac{1}{4},\ \tfrac{1}{2}p - \tfrac{1}{4},\ -\tfrac{1}{6}\right)\\
\mathcal{E}(e_5) &= \left(-p,\ -\tfrac{1}{2}p - \tfrac{1}{4},\ -\tfrac{1}{6}\right)\\
\mathcal{E}(e_6) &= \left(-p,\ -\tfrac{1}{2}p + \tfrac{1}{4},\ -\tfrac{1}{6}\right)\\
\mathcal{E}(e_7) &= \left(p,\ \tfrac{1}{2}p + \tfrac{1}{4},\ -\tfrac{1}{6}\right)\\
\mathcal{E}(e_8) &= \left(p,\ \tfrac{1}{2}p - \tfrac{1}{4},\ \tfrac{1}{6}\right)\\
\mathcal{E}(e_9) &= \left(\tfrac{1}{2}p + \tfrac{1}{4},\ p,\ \tfrac{1}{6}\right)\\
\mathcal{E}(e_{10}) &= \left(\tfrac{1}{2}p - \tfrac{1}{4},\ p,\ -\tfrac{1}{6}\right)\\
\mathcal{E}(e_{11}) &= \left(-\tfrac{1}{2}p - \tfrac{1}{4},\ -p,\ \tfrac{1}{6}\right)\\
\mathcal{E}(e_{12}) &= \left(-\tfrac{1}{2}p + \tfrac{1}{4},\ -p,\ \tfrac{1}{6}\right)
\end{aligned}$$

with $p \in \mathbb{R}$. Given the orientation of the edges in Fig. 8, the relative positions of two Si atoms bonded to the same O atom can be expressed as $\mathcal{E}(e_1) + \mathcal{E}(\bar{e}_i + 1)$ (for odd i). For example, $\mathcal{E}(e_1) + \mathcal{E}(\bar{e}_2) = \left(-\tfrac{1}{2}, -\tfrac{1}{2}, \tfrac{1}{3}\right)$. These vectors are independent from p and therefore the positions of the Si atoms depend only on the setting. For $p = -0.0843$, the embedding is equivalent to the high-temperature quartz structure. For a hexagonal cell ($a = b$, $\gamma = 120^\circ$), the bonds have length $\tfrac{1}{2}[a^2\left(p^2 + \tfrac{1}{4}\right) + (c^2/9)]^{1/2} \simeq 1.545 + 1.98p^2$ for the cell parameters of the high-temperature modification and $p \in [-0.2, 0.0]$.

If only the symmetries corresponding to the low-temperature phase are enforced, $\mathcal{E}$ has four degrees of freedom (p, q, r and s). For e_1 and e_2 the embeddings are

$$\begin{aligned}
\mathcal{E}(e_1) &= (p - q, -q, s)\\
\mathcal{E}(e_2) &= \left(1 - 2q + r + p, -r, s - \tfrac{1}{3}\right)\\
\mathcal{E}(e_1) - \mathcal{E}(e_2) &= \left(q - r - 1, r - q, \tfrac{1}{3}\right).
\end{aligned}$$

Obviously, only the distance along the c axis of the Si atoms is definite. However, the positions of the O atoms are again less constrained than the positions of the Si atoms.

6.7. Garnets

Almandine ($Fe_3Al_2Si_3O_{12}$), a garnet with space group $Ia\bar{3}d$, was chosen for the reason that garnets exhibit rather complex yet highly symmetric structures. During the conversion of the structure, the Fe atoms were considered as not bonded and were therefore removed. The resulting QG has 136 nodes and 192 edges. If only the consistency of the QG is taken into account, its embedding has 405 degrees of freedom as compared to 201 if the centring translation is also included.

Table 4 shows the degrees of freedom an embedding of a garnet QG has if the embedding is constrained by selected sets of automorphisms. For simplicity, the symmetries of an

Table 4
Degrees of freedom for the garnet QG and given sets of automorphisms.

t is the translation centring of the unit cell, *m* is a glide or mirror plane, and 2 and 3 are rotation or screw axes. The notation [*abc*] indicates the orientation of an axis or a plane normal: [100] designates a line parallel to the *a* axis, [110] designates a line parallel to the diagonal in the *ab* plane *etc.*

Automorphisms	Degrees of freedom
1	405
t	201
t, m[100]	100
t, m[110]	100
t, 2[011]	99
t, 2[100]	99
t, $\bar{1}$	90
t, 3[111]	67
t, $\bar{3}$[111]	30
t, 4_1[100]	49
t, $\bar{4}$[100]	48
t, all 2	8
t, all 4_1†	8
t, all $\bar{4}$†	7
t, all m	3
t, all 3	16
t, all 3, all $\bar{3}$	7
t, all 3, all 4_1†	8
t, all 3, all $\bar{4}$†	7
t, all 3, $\bar{1}$	7
t, all 3, all 2	3
All automorphisms	3

embedding of a net instead of the automorphisms are given; rotations and mirror planes may include screw axes or glide planes. (A given automorphism may correspond to several symmetry elements; *e.g.* a parallel screw and rotation axis.) Also, many redundant sets are omitted, as, due to the cubic symmetry of garnet, they constrain $\mathcal{E}$ in similar ways (*e.g.* $\{t, 2[100]\}$, $\{t, 2[010]\}$ and $\{t, 2[001]\}$).

All automorphisms constrain the embedding of the net to various degrees. As for all sets of automorphisms, $\{t, \varphi\}$ constrains $\mathcal{E}$ more than t (see the upper part of Table 4); it can be concluded that no symmetry is implicit. However, if the embedding has at least two perpendicular fourfold rotations (rotoinversions), the threefold rotations in the arrangement typical for a cubic space group are implicit (see the entries in Table 4 marked with a dagger). Therefore, if the unit cell is cubic, a structure with these symmetries has at least the symmetry of $I4_132$ ($I\bar{4}3d$). Contrary to this, an argument relying on group theory only would allow space groups $I4_1/acd$ ($I\bar{4}2d$), also for a cubic unit cell.

In principle, space group $Ia\bar{3}d$ has three cubic *translationengleiche* subgroups. Thus, a displacive phase transition of garnet could lead to a structure with the symmetries of space groups $Ia\bar{3}$, $I4_132$ or $I\bar{4}3d$. All three are possible from the perspective of this article: constraining the QG embedding with the centring translation and all threefold rotations, possibly in combination with other additional symmetries, produces sets of constraints with four different degrees of freedom (16, 8, 7 and 3; see the lower part of Table 4). As the equivalent embeddings have cubic symmetries (due to the presence of threefold rotational axes), these sets must correspond to one of the four possible space groups.

If constrained by all automorphisms, the embeddings $\mathcal{E}$ of edges corresponding to Al—O and Si—O bonds are the permutations of vectors

$$\begin{pmatrix} \pm p \\ \pm q \pm \frac{1}{8} \\ \pm r \end{pmatrix} \quad \text{and} \quad \begin{pmatrix} \pm p \pm \frac{1}{4} \\ \pm q \\ \pm r \end{pmatrix},$$

respectively, with $p, q, r \in \mathbb{R}$. All Si atoms are bonded to Al atoms *via* O-atom bridges. Adding the embeddings of the edges of an O-atom bridge (while respecting their orientations) always results in a definite vector. Therefore, in a fully constrained embedding of a net, the nodes at the ends of the bridges are at definite relative positions (that is, the Si and Al lattices and their relative positions are determined). For an arbitrarily chosen bridge, this is

$$\begin{pmatrix} -p \\ r \\ q - \frac{1}{8} \end{pmatrix} + \begin{pmatrix} -\frac{1}{4} + p \\ -r \\ -q \end{pmatrix} = \begin{pmatrix} -\frac{1}{4} \\ 0 \\ -\frac{1}{8} \end{pmatrix}.$$

For all O-atom bridges, these relative positions are described by permutations of the vector $(0, \pm\frac{1}{8}, \pm\frac{1}{4})$; that is, the cations are at a distance of $[(5^{1/2})/8]a$. From the constraints, here for space reasons, it is evident that a variation of any of the three free parameters would displace the O atoms by the same distance along a line parallel to an axis. To be precise, one third of the O atoms move in the direction of the *a* axis, one third move along the *b* axis and the remaining along the *c* axis. For each atom there exists another atom moving in the inverse

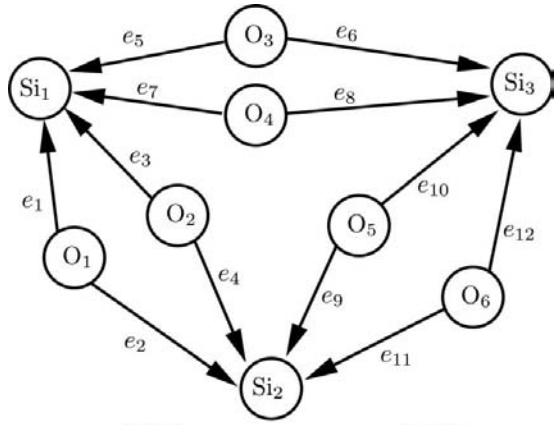

$e_1 = \mathrm{O}_1 \xrightarrow{(0,0,1)} \mathrm{Si}_1$ $\quad e_2 = \mathrm{O}_1 \xrightarrow{(0,0,0)} \mathrm{Si}_2$
$e_3 = \mathrm{O}_2 \xrightarrow{(0,1,1)} \mathrm{Si}_1$ $\quad e_4 = \mathrm{O}_2 \xrightarrow{(-1,0,0)} \mathrm{Si}_2$
$e_5 = \mathrm{O}_3 \xrightarrow{(0,0,0)} \mathrm{Si}_1$ $\quad e_6 = \mathrm{O}_3 \xrightarrow{(0,0,0)} \mathrm{Si}_3$
$e_7 = \mathrm{O}_4 \xrightarrow{(0,-1,0)} \mathrm{Si}_1$ $\quad e_8 = \mathrm{O}_4 \xrightarrow{(0,0,0)} \mathrm{Si}_3$
$e_9 = \mathrm{O}_5 \xrightarrow{(0,0,0)} \mathrm{Si}_2$ $\quad e_{10} = \mathrm{O}_5 \xrightarrow{(0,0,0)} \mathrm{Si}_3$
$e_{11} = \mathrm{O}_6 \xrightarrow{(-1,0,0)} \mathrm{Si}_2$ $\quad e_{12} = \mathrm{O}_6 \xrightarrow{(0,0,0)} \mathrm{Si}_3$

Figure 8
The quartz QG.

direction. Fig. 9 illustrates this for one parameter (see also the supplementary video provided online). Any variation of these parameters preserves the centre of mass of a unit cell. In an embedding with a standard setting, the Al, Si and O atoms must be positioned at the Wyckoff positions 16*a*, 24*d* and 96*h*, respectively.

7. Comparison of the present work with that of Eon (1999)

Eon's work (Eon, 1999) and the work presented here are superficially distinct: Eon uses cycles, co-cycles and projections of the spaces defined by them to consider atom positions in Euclidean space. In contrast, in the present work sums over labels and vectors assigned to edges in cycles and paths are used to consider relative atom positions.

On a closer look, however, similarities become evident:

(*a*) The projection of (co-)cycles is equivalent to the summation on edge embeddings in cycles. The observation by Eon that the sums $\sum n_i c_i$ (where n_i is an integer and c_i are the elements of the co-cycle space) correspond to the demand that an embedding fulfils equation (1); the (integer-valued) sum $\sum_{e\in c} v$ represents the fact that nodes belong to a given lattice.

(*b*) The proof by Eon concerning the relation between the automorphism group of the (unlabelled) QG (without loops and bridges) and the space group of an embedding with maximal symmetry is in many aspects equivalent to the proof given in Thimm & Winkler (2006). This relationship is the basis for the discussion in §4.

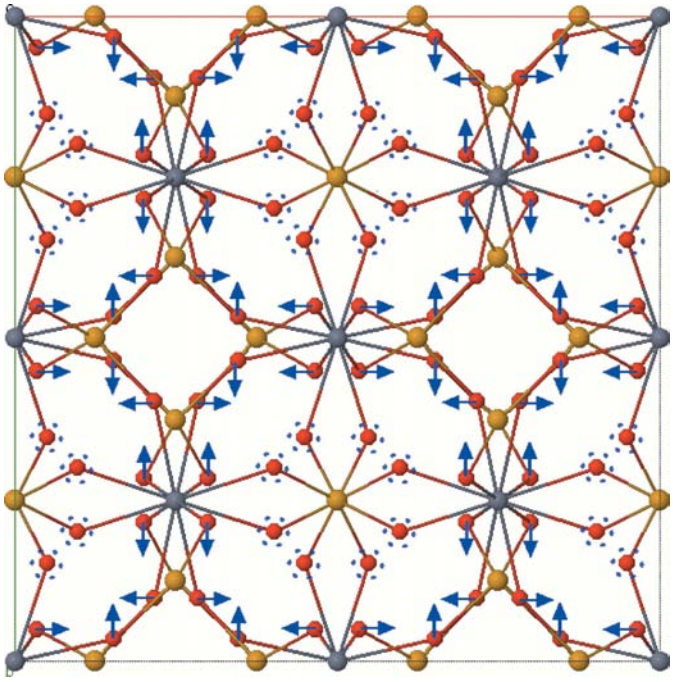

Figure 9
The projection of the garnet structure without cations along the *c* axis. The arrows indicate the changes of the positions of the O atoms for decreasing *q* from the value observed for the almandine structure. O atoms surrounded by dots are displaced perpendicular to the image plane.

(*c*) It is likely that the theory presented here can be expressed using the tools used in Eon's work.

Differences are:

(*a*) Eon demands that in an embedding bonds have comparable lengths and nonbonded atoms are at a minimal distance larger than this. Here, the only demand is that no two nodes are at the same position. Whereas the earlier demand is certainly more realistic in a physical context, solving the corresponding equations is more involved than the equations resulting from the definition used here.

(*b*) The approach using (co-)cycles has the shortcoming that loops and bridges (including singly bonded atoms) cannot be dealt with easily and Eon therefore excludes them. However, many structure types do have QGs with loops or bridges (singly bonded atoms are bonded *via* bridges) – they do not cause difficulties in the approach presented here. As illustrated in §2, bridges have a major impact on the symmetry of a structure and singly bonded atoms cannot be neglected.

(*c*) Although Eon's work does address the relationship between the automorphism group of the QG and the space group of the embedding, he does not push the issue quite as far: no algorithm is given that allows the calculation of the embedding of the QG and the net or that relates nodes to Wyckoff positions.

(*d*) Archetypes have no equivalent here – with the trivial exception that for some QGs the cyclomatic number equals the dimension of its edge labels. Then, the archetype and the net, as defined by the QG, are isomorphic.

(*e*) The proofs relating the automorphism group of the QG and the space group of an embedding have a major difference: Eon's version is valid for archetypes; the proof presented here is valid for an embedding in a space of a given dimensionality (typically smaller than that of the archetype's embedding). A projection of the archetype's embedding into a lower-dimensional space respecting the constraints represented by the edge labels in a QG is not trivial. The example given by Eon uses a graph for which the cyclomatic number is conveniently 3; all connected nets based on the chosen graph are isomorphic. If the cyclomatic number of the base graph is larger than 3, more than one net with isomorphic base graphs exist.

(*f*) In the opinion of the author, the most important difference is the possibility of determining constraints on relative atom positions and associating them with (selected) symmetries.

8. Distances and bond angles *versus* symmetry

One of the referees for this paper posed the question as to whether the symmetry constraints can actually force nodes into physically meaningless positions without causing confusion. An examination of about 80 structures revealed no structure for which this is truly the case [although nets that are impossible to embed such that these trivial constraints are fulfilled greatly outnumber those for which it is possible (Thimm, 2004)]. Only the nets of structures (*e.g.* quartz) that undergo displacive phase transitions can be considered as such

cases. However, the displacements of atoms in such structures are in general minor, and to declare the high-symmetry phases as meaningless is far fetched.

The construction of nets for which a maximal symmetry forces nodes onto such positions, and the difference is not equivalent to one between a high- and low-symmetry 'phase', is surprisingly difficult. A projection along the *c* axis and an oblique view of low-symmetry embedding of such a net is shown in Fig. 10(*a*). This net has nodes of degree one, two and six, a sheet-like structure, and a maximal-symmetry embedding in space group *P*6/*mmm*. This symmetry is only possible if all nodes in a sheet are positioned in a plane. However,

(1) this makes it impossible to maintain the constraint on the distances between bonded atoms and

(2) the embedding has 30° or smaller bond angles.

An out-of-plane arrangement (similar to the one shown in Fig. 10*b*) agrees in terms of distances and bond angles with known structures. This arrangement, though, is incompatible with sixfold rotations and mirror planes parallel to the sheets. The present author knows of no crystal structures with similar characteristics.

Non-confusing embeddings of nets with confusing maximal-symmetry embeddings may be considered to fall in this category. Non-confusing embeddings of nets represented by $\mathbf{Q}^{\mathrm{L}}$ in three-dimensional space can fulfil the constraint on bond lengths and angles, but only if the singly connected nodes are at positions well outside the sheets formed by the other nodes (see Fig. 11). This, however, disallows twofold rotations around axes parallel to the sheet, which can be achieved if all connected nodes are embedded in a plane.

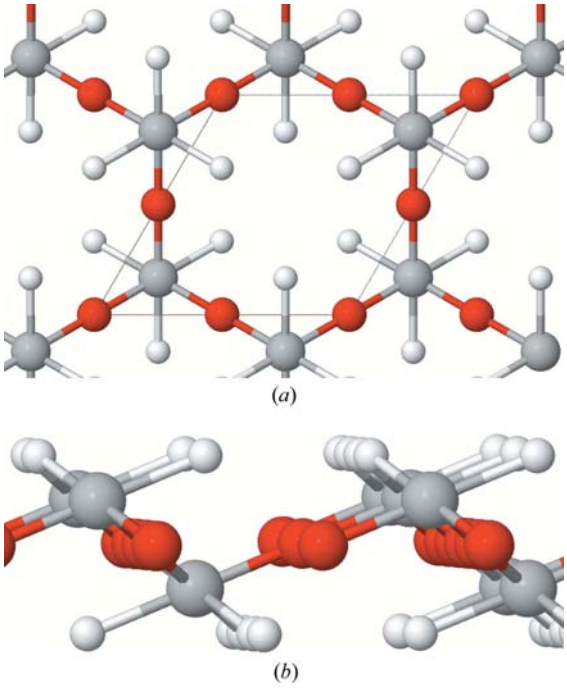

Figure 10
A net for which a maximal-symmetry embedding is physically meaningless yet non-confusing. (*a*) A projection of an embedding with maximal symmetry along the *z* axis. (*b*) An oblique projection perpendicular to the *z* axis of an out-of-plane arrangement with physically reasonable distances between nodes and bond angles.

9. Software

The quotient graphs shown in this paper were created using a modified version of *Jmol*. This version of *Jmol* and software that enables the calculation of QG automorphisms, the establishment and solution of the constraints, and the creation of CIFs for the obtained embeddings can be obtained from the author's web page at http://www.adam.ntu.edu.sg/~mgeorg.

10. Conclusions

An observation of crystal structures and two-dimensional grids shows that for a given topology (connectivity) certain symmetries are forbidden or necessary.

This observation is substantiated by examining how the graph-theoretical equivalents of structures are embedded. This is achieved by defining an embedding of quotient graphs and extending this definition to nets (the graph-theoretical equivalents of structures). Then, for embeddings of a quotient graph, constraints on the relative node positions are proposed which ensure that the embedding of the net possesses a given symmetry and that distinct nodes are at distinct locations. It is shown that if the embedding of a quotient graph fulfils certain conditions, then the embedding of the corresponding net has an equivalent symmetry.

Two two-dimensional examples illustrate the definitions and proposed theorems.

For the halite structure it is shown that imposing a single threefold rotational symmetry leaves one degree of freedom to the structure, whereas an inversion fully defines it and therefore imposes a cubic symmetry (presuming a cubic unit cell). Diamond is cited as an example where, in contrast to halite, the demand for an inversion symmetry does not constrain the structure (that is, all structures with the diamond topology have an inversion symmetry). For the pyrite, quartz and garnet structures it is shown that even the demand for a maximal (cubic) symmetry does not fully constrain the structure and that reduced symmetries have a more or less constraining influence on the structure. However, in all three fully constrained structures, the Fe, Si and Al—Si lattices,

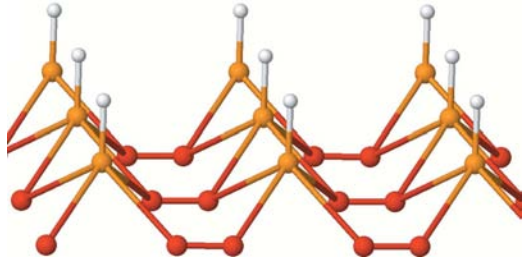

Figure 11
An embedding of $\mathbf{Q}^{\mathrm{L}}$ with reasonable bond angles and distances between nodes.

respectively, are definite, whereas the S and O atoms are free to move.

For the garnet structure it is shown that certain space groups in combination with a cubic cell are forbidden.

Overall, the examples show that an embedded net with a given topology may by default possess a symmetry different from *P*1. Enforcing the presence of some symmetry elements may implicitly include others in excess of those predicted by group theory.

In all the examples examined, the embeddings determined from the automorphisms of the quotient graphs and the structures observed in nature agree well.

A comparison with the approach of Eon (1999) highlights the common aspects and differences of the two approaches. A discussion of whether constraints on distances between atoms and on bond angles result in restrictions on symmetry without confusing nodes shows that, in principle, such restrictions are possible but probably rare for crystal structures.

References

Baburin, I. A. & Blatov, V. A. (2007). *Acta Cryst.* B**63**, 791–802.

Blatov, V. A. (2007). *Acta Cryst.* A**63**, 329–343.

Chung, S. J., Hahn, Th. & Klee, W. E. (1984). *Acta Cryst.* A**40**, 42–50.

Cohen, E. & Megiddo, N. (1991). *Applied Geometry and Discrete Mathematics. The Victor Klee Festschrift*, edited by P. Gritzmann & B. Sturmfels, Vol. 4, pp. 135–146. Rutgers: American Mathematical Society/Association for Computing Machinery.

Delgado-Friedrichs, O. & O'Keeffe, M. (2003). *Acta Cryst.* A**59**, 351–360.

Downs, R. T. & Hall-Wallace, M. (2003). *Am. Mineral.* **88**, 247–250. http://rruff.geo.arizona.edu/AMS/.

Eon, J. G. (1999). *J. Solid State Chem.* **147**, 429–437.

Grosse-Kunstleve, R. W. (1999). *Acta Cryst.* A**55**, 383–395.

Hahn, Th. (1992). Editor. *International Tables for Crystallography*, Vol. A, 3rd ed. Dordrecht: Kluwer Academic Publishers.

Heany, P. J. (1994). *Silica. Physical Behavior, Geochemistry and Materials Applications. Reviews in Mineralogy*, edited by P. J. Heany, C. T. Prewitt & G. V. Gibbs, Vol. 29, pp. 1–40. Washington: Mineralogical Society of America.

Kihara, K. (1990). *Eur. J. Mineral.* **2**, 63–77.

Klee, W. E. (2004). *Cryst. Res. Technol.* **39**, 959–968.

Klein, H.-J. (1996). *Math. Model. Sci. Comput.* **6**, 325–330.

Lutz, H., Himmrich, J., Müller, B. & Schneider, G. (1992). *J. Phys. Chem. Solids*, **53**, 815–825.

Putnis, A. (1992). *Introduction to Mineral Sciences.* Cambridge University Press.

Schumacher, S. (1994). *Periodische Graphen und Beiträge zu ihren Wachstumsfolgen*. PhD thesis, Fakultät für Physik, Universität Karlsruhe, Karlsruhe, Germany.

Thimm, G. (2004). *Z. Kristallogr.* **219**, 528–536.

Thimm, G. (2008). *A Graph Theoretical Approach to the Analysis, Comparison, and Enumeration of Crystal Structures*. PhD thesis, Fachbereich Geowissenschaft, der Johann Wolfgang Goethe Universität in Frankfurt Am Main. http://publikationen.ub.uni-frankfurt.de/volltexte/2008/5723/.

Thimm, G. & Winkler, B. (2006). *Z. Kristallogr.* **221**, 749–758.

Wenk, H.-R. & Bulakh, A. (2004). *Minerals. Their Constitution and Origin.* Cambridge University Press.